

See discussions, stats, and author profiles for this publication at: <https://www.researchgate.net/publication/272128114>

# Pyroelectricity in Nonpolar Directions in Crystals: Enantiomeric Disorder and Surface Wetting in Racemic $\alpha$ -Amino-Acids

ARTICLE in CRYSTAL GROWTH & DESIGN · AUGUST 2014

Impact Factor: 4.89 · DOI: 10.1021/cg5003644

---

CITATIONS

3

READS

23

## 4 AUTHORS:



Eran Mishuk

Weizmann Institute of Science

3 PUBLICATIONS 7 CITATIONS

[SEE PROFILE](#)



Isabelle Weissbuch

Weizmann Institute of Science

113 PUBLICATIONS 3,946 CITATIONS

[SEE PROFILE](#)



Meir Lahav

Weizmann Institute of Science

298 PUBLICATIONS 9,910 CITATIONS

[SEE PROFILE](#)



Igor Lubomirsky

Weizmann Institute of Science

101 PUBLICATIONS 1,112 CITATIONS

[SEE PROFILE](#)

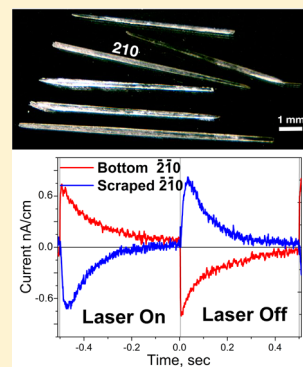
# Pyroelectricity in Nonpolar Directions in Crystals: Enantiomeric Disorder and Surface Wetting in Racemic $\alpha$ -Amino-Acids

Eran Mishuk, Isabelle Weissbuch, Meir Lahav,\* and Igor Lubomirsky\*

Department of Materials and Interfaces, Weizmann Institute of Science, Rehovot 76100, Israel

## S Supporting Information

**ABSTRACT:** Display of pyroelectricity along nonpolar directions of crystals or from surfaces implies structural disorder or presence of polar surface layers. Nonpolar {210} faces of polar DL-alanine crystals display far larger pyroelectric effect than that at the polar {001} faces. Similarly, pyroelectricity is reported from {110} faces of centrosymmetric crystals of DL-aspartic acid. The origin of the disorder is due to an interchange of enantiomers at specific chiral crystal sites as supported by atom–atom potential energy computations and by pyroelectric effect observed on the nonpolar crystals of L-alanine intentionally doped with opposite enantiomers. These results should explain the riddle of the needle-like morphology of DL-alanine. The {100} faces of DL-serine and the {021} faces of DL-glutamic acid monohydrate crystals exhibit pyroelectricity due to surface wetting, whereas pyroelectricity originating from the {210} faces of enantiomerically doped L-alanine crystals could be deciphered as arising both from surface wetting and enantiomeric bulk disorder.



Pyroelectricity is the ability of some crystals to generate spontaneous polarization, detectable by external electric current between two opposing surfaces, when exposed to temperature change.<sup>1</sup> It was generally considered that this property is confined exclusively to the polar directions of 10 out of 32 crystal classes. This rule persisted despite the fact that all crystals, including the centrosymmetric ones, are delineated by 2-D polar surfaces. For a long time, experimental observation of the pyroelectricity associated with surface polarity was thought to be impossible because surface polarization attracts very little external charges (depolarization charge) to be detectable. During the past decade, however, improvement in instrumentation<sup>2</sup> provided means to measure accurately pyroelectric currents of a few picoamperes and pyroelectric coefficients on the order of  $10^{-11}$  C/(cm<sup>2</sup>·K), which is 1:1000 with respect to commercially important materials. This opens a possibility for using the pyroelectric effect as a tool to study the structures of nonpolar surfaces, which delineate crystals in general and wetted surfaces in particular.<sup>3</sup> In addition, this method allows detection of orientational ordering in noncrystalline inorganic materials<sup>4–7</sup> and disorder in organic crystals<sup>8–10</sup> and in racemic compounds in particular, as described in the present study, which is not easily detectable by diffraction techniques.

Recently, we reported surface pyroelectricity emerging from nonpolar wetted layers that delineate the {010} faces of the centrosymmetric crystals of  $\alpha$ -glycine and the {210} faces of the nonpolar crystals of L-alanine (L-Ala).<sup>3</sup> During our attempts to extend these pyroelectric studies to other surfaces of the nonpolar crystals of the amino acids, we discovered the presence of bulk enantiomeric disorder in the polar crystals of DL-Ala and within the centrosymmetric crystals of DL-aspartic acid (DL-Asp). We demonstrate below that this pyroelectricity originates as a result of a partial interchange of enantiomers at

chiral crystal sites. Pyroelectricity was displayed, also, by the nonpolar wetted layer of the centrosymmetric crystals of DL-serine (DL-Ser) and DL-glutamic acid (DL-Glu) monohydrate. Absence of the bulk pyroelectric effect in these crystals implies the absence of “enantiomeric interchange”.

## RESULTS AND DISCUSSION

**Pyroelectricity in DL-Ala Crystals.** DL-Ala crystallizes in the orthorhombic polar  $Pna2_1$  space group assuming a needle-like morphology,<sup>11</sup> as shown in Figure 1a. The crystals grow unidirectionally along the polar  $-c$  direction where the carboxylate ( $CO_2^-$ ) groups are exposed, via a “relay” type mechanism,<sup>12,13</sup> giving rise to well-developed nonpolar {210} side faces, Figure 1b.

Bulk pyroelectric effect was measured along the  $c$ -direction, as depicted in Figure 2a, corresponding to a pyroelectric coefficient of  $(0.5–2) \times 10^{-9}$  C/(cm<sup>2</sup>·K), which was calculated according to eq 2 shown in the Experimental Section.

The symmetry of the DL-Ala crystal implies that no pyroelectricity is anticipated from its nonpolar {210} faces. The packing arrangement at the {210} faces of DL-Ala, however, resemble those of the {210} faces of L-Ala, from which we reported surface pyroelectricity deriving from wetted layers created at these faces.<sup>3</sup> Accordingly, we expected similar surface pyroelectricity from these surfaces, and indeed, these faces display an effect with a pyroelectric constant even greater than that measured along the polar  $c$  direction. Upon heating of the crystals above 100 °C and remeasurement of the pyroelectricity at room temperature, the current remained unchanged, thus

**Received:** March 16, 2014

**Revised:** May 21, 2014

**Published:** June 13, 2014



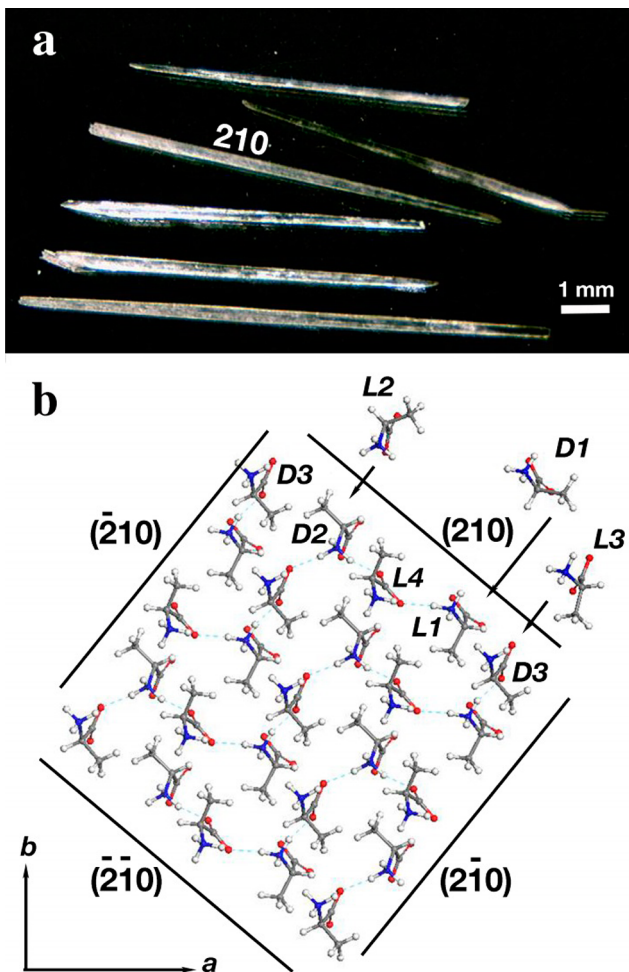


**Figure 1.** DL-Ala (a) needle-like crystals and (b) packing arrangement, viewed along the  $c$ -axis, showing different functional groups exposed at the  $\{210\}$  faces. Enantiomeric molecules, which can occupy sites of opposite handedness, are shown. Color code of the atoms: red, O; blue, N; gray, C; white, H.

demonstrating that this pyrocurrent does not result from water wetting of the surfaces, as in the L-Ala crystals,<sup>3</sup> but from some other reason.

All four  $\{210\}$  faces measured in more than 20 crystals display the same pyroelectric current, positive upon heating, Figure 2b. However, the direction of the current is reversed when  $\sim 0.15$  mm of the crystal is gently removed from the crystal faces by shaving. Such change in sign is indicative of a classical bulk pyroelectric effect deriving from crystalline sectors packed together. The decay of the current is very rapid, Figure 2b, since the crystals are very thin (0.3 mm) and therefore the time required for the heat to diffuse through the whole crystal is very short. For instance, with the L-Ala heat diffusion coefficient of  $0.013 \text{ cm}^2/\text{s}$ ,<sup>14</sup> the time required for the heat to diffuse through a 0.03 cm thick crystal is 0.07 s, which is in accordance with the observed time. Therefore, the crystal can be modeled as composed from four thin sectors for which the pyroelectric coefficient can be calculated from fitting the curve to  $1/t^{1/2}$  dependence, Figure 2b inset.<sup>2</sup>

By taking the slope [ $s = -43.9 \text{ pA}\cdot\text{s}^{0.5}$ ] from the plot in Figure 2b inset and considering that the substrate is made of brass [ $B = 3.01 \times 10^{-5} \text{ K}\cdot\text{s}^{2.5}/\text{kg}$ ] (see Experimental Section), we find that the pyroelectric current corresponds to a

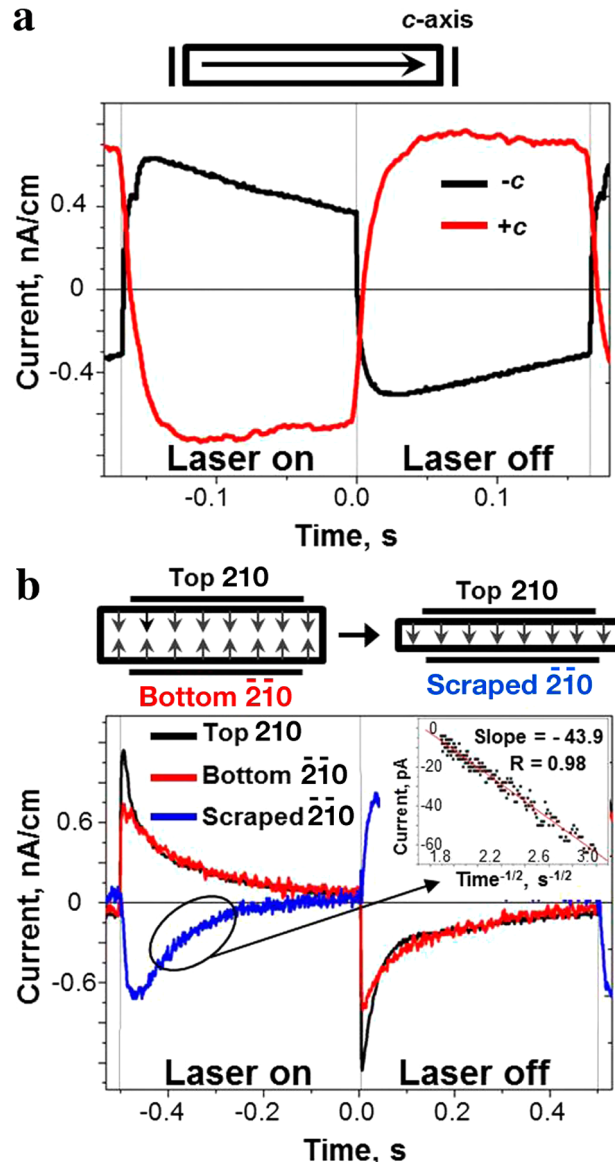


**Figure 2.** (a) In-plane pyroelectric measurement of a DL-Ala crystal along the polar  $c$  direction. Flipping the current sense of  $\pm c$ -directions indicates a bulk pyroelectric effect typical to such polar crystals. (b) Pyroelectric measurement at the expressed  $\{210\}$  faces of a DL-Ala crystal (thickness 0.3 mm) showing the same current direction (red and black curves). When one of the  $\{210\}$  faces is scraped (blue curve) to remove material to about half the crystal thickness, the sense of the current is reversed. Inset, Plot of the current vs  $1/t^{1/2}$  of the marked part of current decay in blue.

pyroelectric coefficient of  $-2.1 \times 10^{-8} \text{ C}/(\text{cm}^2\cdot\text{K})$ . The pyroelectric coefficients of these sectors are at least an order of magnitude higher than those measured along the polar  $c$ -direction of DL-Ala or of LiTaO<sub>3</sub> crystals used for high-end commercial pyroelectric detectors.

The origin of the pyroelectricity at the nonpolar sectors of an ordered crystal cannot be attributed to small deviations of the polar axis away from the  $c$ -direction since the pyroelectric effect in the [210] direction is at least 1 order of magnitude higher than the pyroelectric effect along the polar direction. Moreover, the pyroelectric effect on the opposite  $\{210\}$  faces has the same sign implying that in these directions the crystal consists of at least two sectors with opposite polarity. On the basis of these

findings we must conclude that the sectors responsible for the pyroelectric effect in these directions have reduced symmetry. The origin of polarity at the {210} faces may arise either from some unidentified chemical impurity that was occluded in the crystal and reduces its symmetry or possibly from enantiomeric self-poisoning when an enantiomer at a specific chiral site is replaced by one of opposite handedness.<sup>15,16</sup> The decrease in bulk ordering might occur when molecules have no time to equilibrate into their ordered state during crystal growth. The option of unidentified contaminants was rigorously eliminated by using very pure DL-Ala from different sources. Furthermore, crystals were grown from racemic mixtures of the two enantiomers, which are shown below to be free from unidentified contaminants by pyroelectric measurements. Therefore, we conclude that the observed pyroelectricity at the nonpolar faces of DL-Ala originates from cross-enantiomeric exchange.

The pyroelectric effect shows full reversibility with respect to heating and cooling. Upon heating, it increases in the [210] nonpolar directions, Figure 3a, but it decreases in the polar

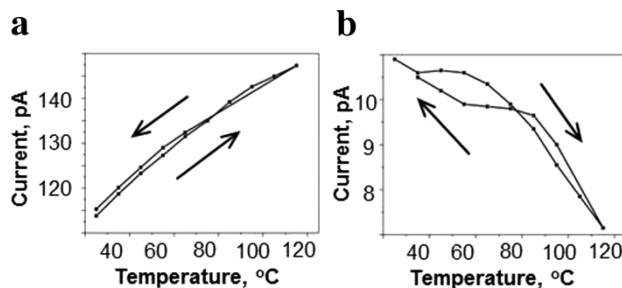


**Figure 3.** Temperature dependence of the current generated (a) from the {210} faces of DL-Ala crystal indicating that upon heating the current increases and upon cooling it fully reversibly decreases and (b) from the {001} polar direction of DL-Ala crystals. Some hysteresis between heating and cooling is due to thermal inertia of the heating stage, which is more pronounced due to large distance between the contacts (>5 mm).

[001] direction of the crystal, Figure 3b. This puzzle of the different behavior of the pyroelectricity along the polar and nonpolar directions can be settled if we take into account the thermal expansion properties of DL-Ala crystals upon heating. Thermal expansion coefficients of DL-Ala in various crystallographic directions were reported as  $7.5 \times 10^{-5}$ ,  $(3.8-5) \times 10^{-5}$  and  $-2.25 \times 10^{-6}$  along *a*, *b*, and *c* crystal axes, respectively.<sup>17,18</sup> Whereas the *c* direction is contracting, the *a*- and *b*-directions are expanding. Crystal contraction along the *c* direction can lead to hardening of the polarization change in this direction, which has negative influence on the pyroelectric effect. Crystal expansion, on the other hand, gives rise to more degrees of freedom, implying that the dipoles can rotate and vibrate more easily, thus enhancing the pyroelectric effect upon heating along the [210] directions. Such a mechanism might also rationalize the display of the huge pyroelectric coefficient along the [210] directions.

More direct demonstration of the proposed “cross-inhibition mechanism” is provided also by comparative studies of the corresponding pure L- and D-Ala enantiomorphs, Figure 4a (orthorhombic space group  $P2_12_12_1$ ), which display packing similarities with the DL-Ala crystals. The four molecules that reside near the {210} faces shown in Figure 4d resemble those found at the {210} faces of the DL-Ala, albeit they are of the

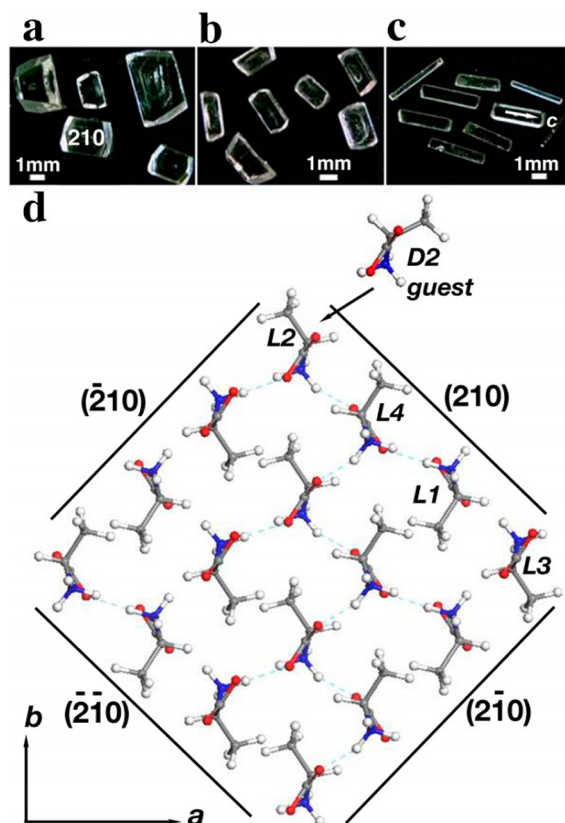


**Figure 4.** L-Ala crystals grown from (a) the enantiomerically pure solution and (b) 5% and (c) 10% D-Ala in L-Ala solution, displaying developed {210} faces. The crystals show elongation along the *c* direction as the amount of the opposite enantiomer increases. (d) Packing arrangement of L-Ala crystal, viewed along the *c* direction, showing different functional groups exposed at the {210} faces. Color code of the atoms: red, O; blue, N; gray, C; white, H.

same handedness. Although these crystals grow from a single enantiomer, they can be contaminated intentionally by the opposite enantiomer, thus inducing bulk pyroelectricity resulting solely from the created enantiomeric disorder.<sup>13,19,20</sup> Crystals of L-Ala grown in the presence of 5–10% D-Ala present in the L-Ala solution exhibit an elongated morphology, as depicted in Figure 4b,c. In comparison to the pure crystals, the elongation occurs progressively along their *c*-direction leading to pronounced expression of the {210} faces. The occluded amount of the enantiomeric contaminant is minute, ~0.3 wt %, as detected by deuterium NMR analysis performed on dissolved D-Ala single crystals grown in the presence of trideuturated L-Ala (see Supporting Information).

In contrast to pure L-Ala crystals that do not display pyroelectricity after their heating above 100 °C,<sup>3</sup> doped L-Ala crystals display bulk pyroelectricity. For the latter crystals, the pyrocurrent measured from two opposite {210} faces has opposite sign, indicating a bulk effect, Figure 5a. The time dependence of the current is also a representative for the presence of a bulk effect since after some decay the pyroelectric current stabilizes at a constant value, Figure 5a. The pyroelectric signal in the first heating–cooling cycle of a freshly doped L-Ala crystal (Figure 5b) shows that during heating the current decreases until 70 °C due to disordering of dipoles but starts to increase as the water effect (which contributes negatively to the total pyrosignal) decreases. Upon cooling back to room temperature, the signal increases

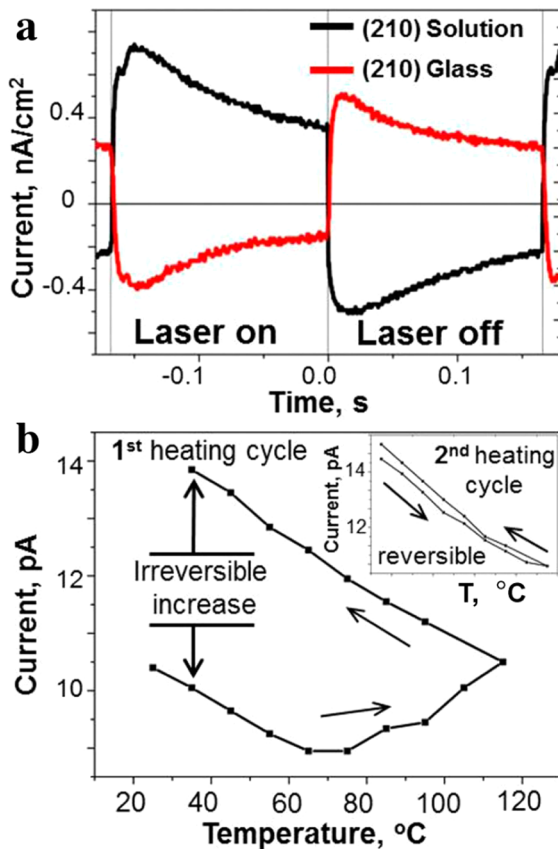


**Figure 5.** (a) Pyroelectric current generated by a D-Ala doped L-Ala crystal (10% in solution) of 1 mm thickness. The flipping in the current sign from opposite faces indicates a bulk pyroelectric effect. (b) Temperature dependence of the current generated from (210) face of a fresh D-Ala doped L-Ala crystal. Inset, second heating–cooling cycle of the same crystal.

irreversibly by ~30%. After removal of water, all subsequent heating–cooling cycles are fully reversible, deriving solely from the crystal's bulk polarization, Figure 5b, inset.

This bulk polarization effect is in keeping with the occlusion of the opposite enantiomer within the crystalline lattice, as independently demonstrated by inserting trideuterated-L-Ala

within crystals of D-Ala as confirmed by deuterium NMR measurements.

No pyroelectric effect was found along the *c*-direction of the crystal implying that the doped crystal is a conglomerate composed from two pairs of polar sectors of opposite polarities coherently compounded, which preserve the original 2<sub>1</sub>-fold symmetry of the pure crystal.

In summary, all the above experiments confirm that crystals of DL-Ala are composed from four enantiomerically disordered sectors, of symmetry *P*1 coherently compounded. All four sectors assume the same sense of polarity, and thus the overall symmetry of the conglomerate preserves the original symmetry, *Pna*2<sub>1</sub>, of the crystal, as anticipated from the Newman–Curie symmetry principle.

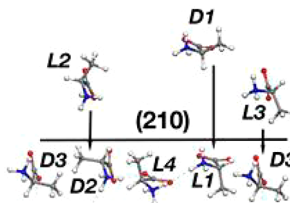
The presence of enantiomeric disorder in both the DL-Ala and the doped L-Ala crystals is further supported by atom–atom potential energy calculations.

**Modeling Cross-Enantiomeric Site Substitution in DL-Ala Crystals by atom–Atom Potential Energy Computations.** Two pairs of Ala enantiomers reside at the {210} faces of the crystal, Figure 1b. The relative layer, attachment, and binding energies (see Supporting Information) were calculated for each site to reflect the docking and occlusion during subsequent growth when a regular host molecule was replaced with a guest molecule of opposite chirality. Replacement of the host by a guest molecule was performed via an interchange of either (i) H with CH<sub>3</sub>, (ii) H with NH<sub>3</sub><sup>+</sup>, (iii) H with CO<sub>2</sub><sup>−</sup>, or (iv) NH<sub>3</sub><sup>+</sup> with CO<sub>2</sub><sup>−</sup> groups. The results are summarized in Table 1.

The molecular modeling results show that docking of an Ala molecule of opposite chirality may occur easily with almost no energetic penalty at sites 1, 2 and 3, just by the interchange of the (C<sub>α</sub>)H atom with the CH<sub>3</sub> group ( $\Delta E_l$  of +0.6, −1.8, and −0.7 kcal/mol, respectively, see Table 1). In this manner, the charged NH<sub>3</sub><sup>+</sup> and CO<sub>2</sub><sup>−</sup> groups, defining the polar crystal *c* direction remain unchanged. Incorporation of the opposite enantiomer at site 4 would force the CH<sub>3</sub> group to point into the bulk giving rise to high steric repulsion. Therefore, the energetic penalty,  $\Delta E_b$ , increases by +5.4 kcal/mol.

Site 2 is the most favorable site for interchange between molecules of opposite handedness, since the (C<sub>α</sub>)H atom of the D-Ala host molecule is emerging from the (210) plane. The steric repulsion of the emerging CH<sub>3</sub> group of an L-Ala docked

**Table 1. Summary of Calculated Relative Energies<sup>a</sup> Representing the Energetic Cost for Docking and Occlusion of an Enantiomer of Opposite Handedness in Any of the DL-Ala Host Crystal Sites at the (210) Crystal Face**



site no. (Ala host)	(Ala guest)	H vs CH <sub>3</sub>			H vs NH <sub>3</sub> <sup>+</sup>			H vs CO <sub>2</sub> <sup>−</sup>			NH <sub>3</sub> <sup>+</sup> vs CO <sub>2</sub> <sup>−</sup>		
		$\Delta E_l$	$\Delta E_{att}$	$\Delta E_b$	$\Delta E_l$	$\Delta E_{att}$	$\Delta E_b$	$\Delta E_l$	$\Delta E_{att}$	$\Delta E_b$	$\Delta E_l$	$\Delta E_{att}$	$\Delta E_b$
1 (L)	(D)	+0.6	+8.1	+8.7	+3.6	+9.8	+13	+7.8	+24	+31	+37	+42	+79
2 (D)	(L)	−1.8	+8.1	+6.3	+2.6	+6.7	+9.3	+14	+22	+36	+13	+69	+82
3 (D)	(L)	−0.7	+8.0	+7.4	+2.7	+9.7	+12	+12	+24	+36	+37	+43	+80
4 (L)	(D)	+5.4	+18	+23	+4.5	+9.6	+14	+3.5	+17	+20	+56	+46	+102

<sup>a</sup>Layer energy,  $\Delta E_l$ ; attachment energy,  $\Delta E_{att}$ ; binding energy,  $\Delta E_b$ . All energies reported in kcal/mol. Site numbering is shown.

in this site is only minor. No large energetic penalty is anticipated by enantiomeric exchange in site 3 since both ( $C_\alpha$ ) H atom and  $\text{CH}_3$  group are pointing into the crystal and their interchange would not cause high steric repulsion. However, the positive relative binding energy of +6.3 and +7.4 kcal/mol at sites 2 and 3, respectively, imply that such enantiomeric exchange may occur in small amounts. Docking of an enantiomer in a site of opposite chirality via the interchange of the ( $C_\alpha$ )H with the  $\text{NH}_3^+$  or the  $\text{CO}_2^-$  group is not favorable due to the energy loss of hydrogen bonding. However, the lowest but positive relative binding energy (+9.3 kcal/mol) is at site 2 only for the interchange between ( $C_\alpha$ )H with the  $\text{NH}_3^+$ .

**Molecular Modeling of Cross-Enantiomeric Site Substitution in L-Ala Crystals.** The results for the relative layer, attachment and binding energies that provide an estimate for the interaction of a dopant D-Ala molecule occupying any of the L-Ala crystal host sites at the (210) face are summarized in Table 2. Such occlusion is performed via the interchange between either H and  $\text{CH}_3$  or H and  $\text{NH}_3^+$  groups, at each site labeled according to the numbering in Table 2.

**Table 2. Summary of Calculated Relative Energies<sup>a</sup>**  
Representing the Energetic Cost for Docking and Occlusion of a D-Ala Molecule in Any of the L-Ala Host Crystal Sites at the (210) Crystal Face

site no. L-Ala host	H vs $\text{CH}_3$			H vs $\text{NH}_3^+$		
	$\Delta E_l$	$\Delta E_{\text{att}}$	$\Delta E_b$	$\Delta E_l$	$\Delta E_{\text{att}}$	$\Delta E_b$
1	+5.0	+25	+30	+6.6	+6.3	+13
2	+1.9	+6.1	+8.0	+8.5	+6.2	+15
3	+24	+30	+54	+18	+6.3	+24
4	+4.8	+6.1	+10.9	+13	+6.3	+19

<sup>a</sup>Layer energy,  $\Delta E_l$ ; attachment energy,  $\Delta E_{\text{att}}$ ; binding energy,  $\Delta E_b$ . All energies reported in kcal/mol.

The results show that the lowest energetic cost for docking a molecule of opposite chirality is at site 2 where both ( $C_\alpha$ )H and  $\text{CH}_3$  group are emerging from the (210) plane,  $\Delta E_l = 1.9$  kcal/mol, similar to site 2 in the DL-Ala crystal. Upon exchange of the ( $C_\alpha$ )H atom with the  $\text{CH}_3$  group, the amount of steric disturbance is minor relative to the other sites and there is no loss of hydrogen bonding. Moreover, the relative attachment energy,  $\Delta E_{\text{att}} = 6.1$  kcal/mol, indicates a relative easy incorporation of the D-Ala during crystal growth. This preferential occlusion of the opposite enantiomer is akin to that in the DL-Ala crystal since the packing arrangement at the (210) surface layers are similar in L- and DL-Ala crystals.

**Pyroelectricity in the Crystals of DL-Asp, DL-Ser, and DL-Glu Monohydrate.** On the basis of the above findings, we analyzed the presence of enantiomeric cross-exchange and the presence of polar wetted layer in the crystals of DL-Asp, DL-Ser, and DL-Glu· $\text{H}_2\text{O}$ .

**DL-Aspartic Acid.** Monoclinic centrosymmetric crystals of DL-Asp, space group C2/c, with prismatic morphology delineated

by well-developed {110} faces were obtained by slow cooling from 50 to 30 °C. One out of the four {110} crystal faces that was lying on the glass/solution interface has a hole differentiating it from the rest. The packing arrangement and morphology of the crystals are shown in Figure 6a,b.

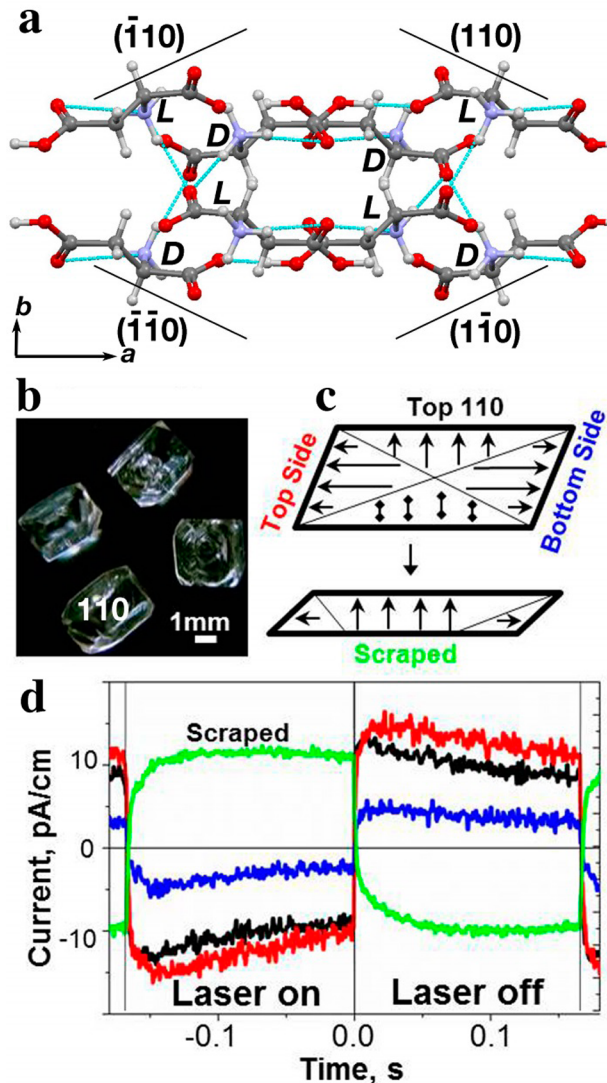
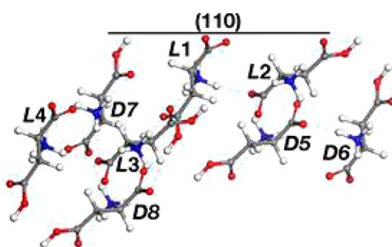


**Figure 6.** DL-Asp crystals: (a) Packing arrangement viewed along the *c* axis. Color code of the atoms: red, O; blue, N; gray, C; white, H. Chirality and site numbering are shown at the (110) face for the atom–atom potential energy calculations. (b) Crystals grown from aqueous solutions displaying well-developed {110} faces. (c) Polarization profile, as assumed by the pyroelectric measurement in panel d showing a crystal composed from sectors of opposite polarity. (d) Pyroelectric measurements of DL-Asp crystal showing the same current direction upon heating fresh {110} faces (red, black, and blue curves). Upon removal of about half of the crystal by shaving, there is a change in current sign (green curve), indicative of bulk pyroelectric effect.

According to the packing arrangement, at the {110} crystal faces, the four L-Asp molecules have their  $C_\alpha$ -H vector pointing toward the +*b* direction, and by symmetry, the D-Asp molecules have their  $C_\alpha$ -H vector pointing toward the -*b* direction. Thus, at the (110) face, the L-Asp molecules have an emerging  $C_\alpha$ -H vector, whereas the D-Asp molecules have their  $C_\alpha$ -H vector buried into the surface. Such orientation of the molecules with regard to the faces might provide the

**Table 3. Summary of Calculated Relative Energies<sup>a</sup> Representing the Energetic Cost for Docking and Occlusion of (a) a D-Enantiomer Molecule in Any of the L-Asp Host Crystal Sites and (b) an L-Enantiomer Molecule in Any of the D-Asp Host Crystal Sites at the (110) DL-Asp Crystal Face**



site no., L-Asp host	(a) D-Asp as Guest								
	H vs CH <sub>2</sub> COOH			H vs NH <sub>3</sub> <sup>+</sup>			H vs CO <sub>2</sub> <sup>-</sup>		
	ΔE <sub>l</sub>	ΔE <sub>att</sub>	ΔE <sub>b</sub>	ΔE <sub>l</sub>	ΔE <sub>att</sub>	ΔE <sub>b</sub>	ΔE <sub>l</sub>	ΔE <sub>att</sub>	ΔE <sub>b</sub>
1	+7.6	+92	+100	+8.8	+13	+22	+2.8	+34	+37
2	+10	+13	+23	+0.13	+13	+13.1	+49	+37	+86
3	-1.0	+30	+29	+5.6	+13	+19	+14	+38	+52
4	+18	+65	+83	+10	+13	+23	+9.5	+36	+46

site no. D-Asp host	(b) L-Asp as Guest						
	H vs NH <sub>3</sub> <sup>+</sup>			H vs CO <sub>2</sub> <sup>-</sup>			
	ΔE <sub>l</sub>	ΔE <sub>att</sub>	ΔE <sub>b</sub>	ΔE <sub>l</sub>	ΔE <sub>att</sub>	ΔE <sub>b</sub>	
5	-2.4	+13	+10.6	+114	+38	+152	
6	+24	+13	+37	+75	+37	+112	
7	+14	+13	+27	+0.8	+11.7	+12.5	
8	+16	+13	+29	+7.6	+37	+45	

<sup>a</sup>Layer energy, ΔE<sub>l</sub>; attachment energy, ΔE<sub>att</sub>; binding energy, ΔE<sub>b</sub>. All energies reported in kcal/mol.

ground for an enantiomeric exchange, resulting in enantiomeric disorder that might be detected by the pyroelectric measurements.

The pyromeasurements showed the same negative current generated upon heating from the three {110} faces pointing toward the solution, Figure 6d. The pyroelectric coefficient of  $(0.5-3) \times 10^{-11}$  C/(cm<sup>2</sup>·K) depends on the growth conditions, in particular the cooling rate of the solution during crystal growth. Crystals from different sources of high purity were used in the pyroelectric measurements excluding the presence of an unidentified contaminant. These results imply that the origin of this pyroelectricity might arise either from wetted layers of the crystal faces or from a conglomerate of sectors enantiomerically self-contaminated. The possible effect of surface wetting was eliminated since the heat dissipation is not following the  $1/t^{1/2}$  rule as attributed to the hydrated thin layers. Furthermore, the magnitude of the current was preserved reversibly upon heating/cooling cycles from room temperature to 100 °C. Consequently, the second assumption of a hybrid crystal structure is supported by changes in the current sign when some material was removed by scraping any of the {110} faces, Figure 6c,d, green curve.

The calculated relative layer, attachment, and binding energies, ΔE<sub>l</sub>, ΔE<sub>att</sub>, and ΔE<sub>b</sub>, for D-Asp enantiomer docked on the (110) face in a host L-Asp site and for L-Asp enantiomer docked in a host D-Asp site in each of the corresponding four symmetry-related sites are given in Table 3a,b corresponding to the site numbering shown.

According to the computational results in Table 3a, docking a “wrong” enantiomer via the interchange between the (C<sub>α</sub>)H atom and the CH<sub>2</sub>CO<sub>2</sub>H group is barely acceptable only in site L3 with a small energetic advantage of ΔE<sub>l</sub>=-1.0 kcal/mol; however the occlusion of the guest requires a very high

energetic cost in binding energy, ΔE<sub>b</sub> = +29 kcal/mol, making such enantiomeric disorder improbable. For site L2, ΔE<sub>b</sub> = 23 kcal/mol is somewhat lower, but ΔE<sub>l</sub> is very high, +10 kcal/mol, making this site also improbable for this type of enantiomeric disorder.

The enantiomeric disorder via the interchange between the NH<sub>3</sub><sup>+</sup> and the CO<sub>2</sub><sup>-</sup> groups is improbable, in general, since it would break the intermolecular H-bonding network, and such computations were not performed. However, one can envisage a partial break of the intermolecular H-bonds, when enantiomeric disorder would occur via the interchange between the (C<sub>α</sub>)H atom and either the NH<sub>3</sub><sup>+</sup> or the CO<sub>2</sub><sup>-</sup> groups.

**Pyroelectricity in DL-Ser and DL-Glu Monohydrate Crystals.** DL-Ser (monoclinic P2<sub>1</sub>/a space group) crystallizes by slow evaporation from aqueous solution in a morphology expressing large {100} faces, where the polar groups are exposed, and small {011} and {110} side faces (Figure 7a,b).<sup>21</sup> Pyroelectricity from hydrated layers at the {100} crystal faces was determined as follows.

Upon laser irradiation, the {100} faces of DL-Ser crystals display a negative pyroelectric current (Figure 7c). The rapid decay of the current is following the  $1/t^{1/2}$  rule implying that the current is generated by a pyroelectric layer that is confined near the surface, Figure 7c, inset. The heating or cooling cycles of the crystals below 45 °C are reversible. By contrast, crystal heating above 45 °C results in an irreversible decrease of current, Figure 7d, and above 115 °C, the current vanishes. Consequently, the pyroelectricity originates from hydrated layers that can be removed by heating the crystals.

Orthorhombic DL-Glu monohydrate crystals (space group Pbc<sub>a</sub>) grown from aqueous solution appear as elongated prisms, Figure 8a, with {021} side faces. The packing arrangement

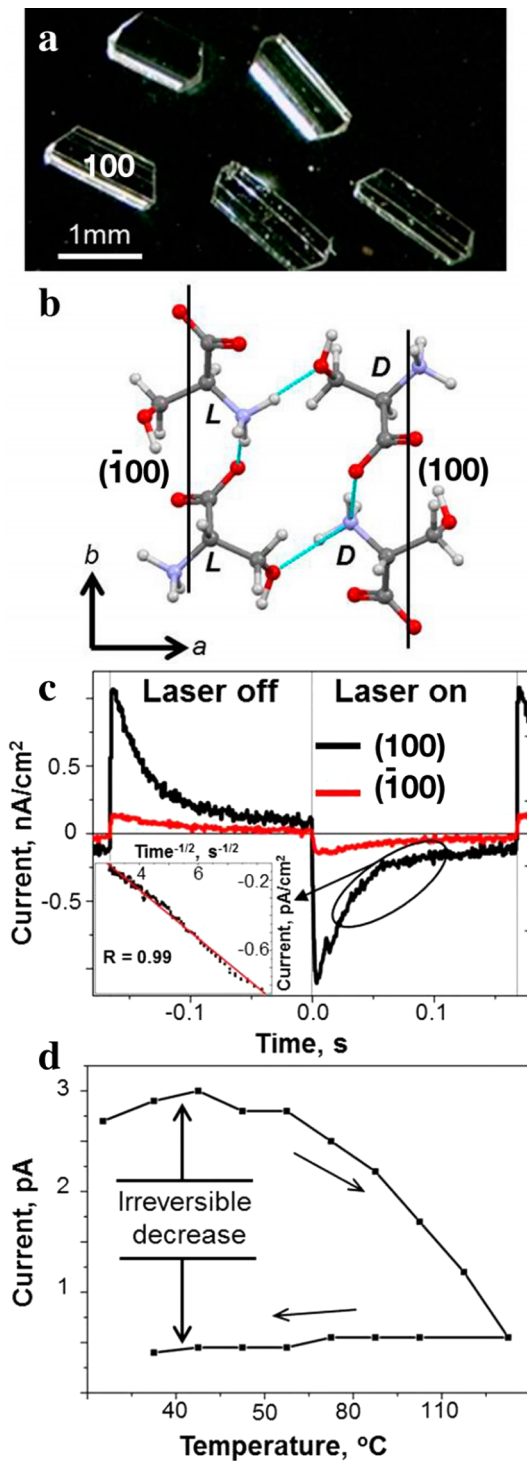


**Figure 7.** (a) DL-Ser crystals showing well-developed  $\{100\}$  faces. (b) Packing arrangement of DL-Ser viewed along the  $c$ -axis. The  $(C_a)H$  atom of the molecules assumes an in-plane orientation with respect to the  $\{100\}$  planes. (c) Pyroelectric measurement of a DL-Ser crystal, 0.4 mm thickness. The current generated from opposite  $\{100\}$  faces has the same direction, negative upon heating with the laser. Inset shows a plot of the current vs  $1/t^{1/2}$ . (d) Temperature dependence of the pyroelectric current.

viewed along the  $a$ -axis illustrates the COOH groups and water molecules exposed at the  $\{021\}$  planes, Figure 8b.

The crystals display a very weak characteristic surface pyroelectricity of the hydrated faces and characteristic

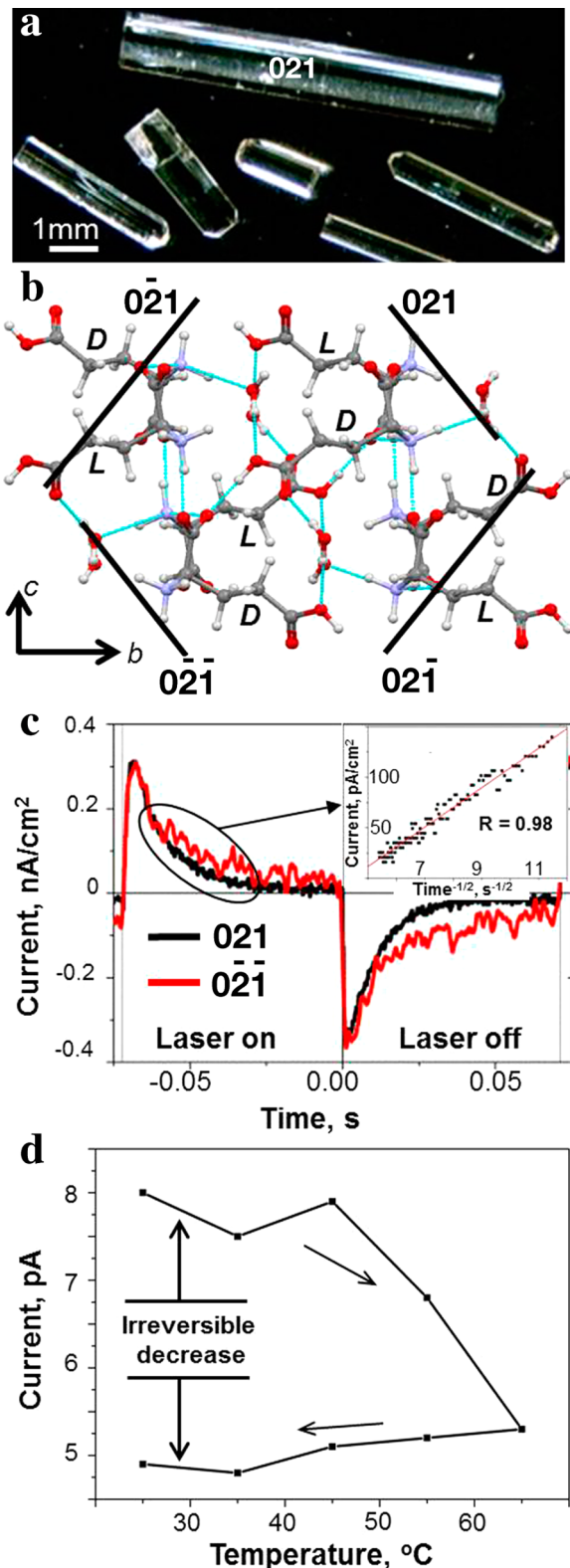


**Figure 8.** (a) DL-Glu monohydrate elongated prisms showing well developed  $\{021\}$  faces as grown from aqueous solution. (b) Packing arrangement of DL-Glu monohydrate crystal illustrating functional groups exposed at the  $\{021\}$  faces. (c) Pyroelectric measurement of a DL-Glu monohydrate crystal, 0.4 mm thickness. The current generated from opposite  $\{021\}$  faces is in the same direction, positive upon heating with the laser. Inset shows a plot of the current vs  $1/t^{1/2}$ . (d) Temperature dependence of the pyroelectric current.

quadruple-like pyroelectric behavior, where the pyroelectricity from the two enantiotopic faces is of the same sign (Figure 8c). The current decays rapidly with  $1/t^{1/2}$  dependence (Figure 8c, inset), implying that the current originates from a pyroelectric layer near the surface. Since the crystal is a hydrate, heating it without phase transition is only possible until 70 °C. An irreversible decrease of the pyrocurrent is observed in keeping with the removal of the bound water, Figure 8d.

Interestingly, the sense of polarity of the thin wetted layers in this crystal is opposite from those found previously in  $\alpha$ -glycine, L-Ala, and DL-Ser crystals, implying that these water molecules are bound to the crystal faces and create polar thin films, which are composed from hydrated amino acid molecules and water layers arranged in a polar configuration.

We conclude that there is no detectable enantiomeric disorder in these crystals. Instead, after crystal growth these faces are delineated by ordered polar wetted films. The pyroelectric method turns to be a most sensitive method to probe such wetted layers since, as proposed by Cowin et al.,<sup>22</sup> water molecules arranged in a polar configuration assume a very high pyroelectric coefficient like that of  $\text{Pb}(\text{Zr}, \text{Ti})\text{O}_3$  ( $\sim 10^{-8}$  C/(cm<sup>2</sup>·K)).

## CONCLUSIONS

Pyroelectricity was generally considered to occur along the polar directions of the polar crystals. However, it turned out that pyroelectricity can provide also information about the occurrence of bulk structural disorder or the presence of thin hydrated polar films that delineate nonpolar crystals of the amino acids. By applying this method, we determined that the crystals of DL-Ala and DL-Asp display enantiomeric disorder. On the other hand, the origin of the pyroelectricity found in the crystals of DL-Ser and DL-Glu monohydrate is due to the presence of thin hydrated films that delineated their surfaces. Furthermore, the origin of the pyroelectricity obtained from the intentionally enantiomerically doped crystals of L- or D-Ala was demonstrated to emerge both from bulk disorder and from the presence of a wetted surface. The mode of the interchange between the enantiomers is supported by atom–atom potential energy computations. Since both the degree of disordering and the degree of wetting are kinetic processes the pyroelectric measurements can provide information regarding the history of the crystal growth, as shown for the DL-Asp crystals.

Surprisingly, the pyroelectricity along the nonpolar {210} faces of DL-Ala crystal exceeds by at least 1 order of magnitude that measured along the polar *c*-axis of the crystal. Such substantial magnitude of the pyroelectric effect implies that this pyroelectricity does not originate solely from the chiral molecules that had occupied sites of opposite handedness in the crystal but also from the local distortions that such interchange introduces by displacing neighboring host molecules from their lattice positions and presumably aligning them in a polar configuration.<sup>23</sup> The presence of such disorder implies that each enantiomer of Ala and Asp can operate as a “tailor-made” inhibitor of growth of those faces and convert the host crystal into a conglomerate of sectors, as demonstrated previously for other contaminants, which are added deliberately to the solutions of the growing crystals.<sup>8–10,24–29</sup> Enantiomeric cross-inhibition together with the operation of the “relay”-type mechanism, which was previously proposed,<sup>12</sup> explains the needle-like morphology of the DL-Ala crystals. The intrinsic disorder structures of the DL-Ala may also rationalize the results reported by Han et al.<sup>19</sup> that the growth of the DL-Ala at low

supersaturation conditions is thicker, presumably comprising lower degree of enantiomeric disorder.

The detection of the polar hydrated faces might provide an experimental demonstration of the role played by water in expressing the size of these faces during their growth.<sup>30,31</sup>

It has also been suggested in previous studies that the nuclei of crystals at the onset of crystallization resemble in structure that of the mature crystals in which they evolve. Therefore, poisoning of certain surfaces of the crystals is anticipated to affect also the kinetic growth of nuclei of similar structures and morphologies and delay or even prevent their conversions into crystals.<sup>16</sup> Kinetic delay in the nucleation of the DL-Asp might be envisaged by the occurrence of such mechanism, since it may contribute to the observed spontaneous resolution of this system when the compound is at conditions away from equilibrium or in the presence of a small excess of one of the enantiomers.<sup>31–33</sup>

Finally the scope of “surface pyroelectricity” as a possible tool for probing the organization and dynamics of water and other polar molecules on rough surfaces other than amino acids is under current investigation.

## EXPERIMENTAL SECTION

**Crystal Growth.** All the commercial materials were used as received. Pure crystals of L-Ala, DL-Ala, DL-Ser, and DL-Glu monohydrate and mixed crystals of L-Ala doped with D-Ala were grown by slow evaporation method from aqueous solutions at 25 °C, and the crystals of DL-Asp were obtained by slow cooling from initial temperature of 50 °C in a clean room environment. Large transparent single crystals were chosen, washed in water, and dried. The crystalline structure was verified and their major faces were indexed with Ultima-III (sealed X-ray tube, Cu anode, 3 kW, RIGAKU, Japan) X-ray diffractometer. More details on crystal growth are given in the Supporting Information.

**Pyroelectric Measurements.** Pyroelectricity was measured by the periodic temperature change technique (modified Chynoweth method,<sup>2,34</sup> Figure 9), which utilizes an 800 mW laser (rise time,

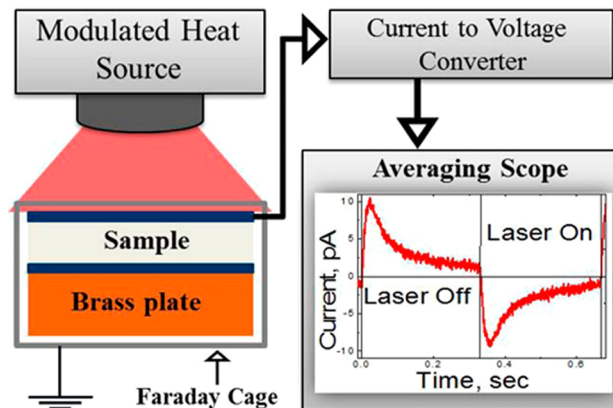


Figure 9. Schematic illustration of the modified Chynoweth method for pyroelectric measurement.

2.5 ms; wavelength, 1.38 μm) that is TTL-modulated by a DG4062 RIGOL waveform generator and produces a heat flux of 3.9–6.9 W/cm<sup>2</sup>. The generated current was measured by low impedance (<10 kΩ at 10<sup>9</sup> V/A and <500 Ω at 10<sup>8</sup> V/A) variable gain low noise current amplifier DLPCA-200 (Femto Ltd.) and recorded with a RIGOL DS2072 digital averaging scope. The sample is located inside a Faraday chamber having a slit for the laser beam and light absorbing inner walls. The contacts of the sample were prepared by fast drying silver paint (5–50 μm) and darkened by black carbon paste or a black

marker for absorption of the laser irradiation. The contacts are completely opaque, providing heat diffusion exclusively from the surface. The thermal diffusion time through the thickest contact was tested with a LiTaO<sub>3</sub> single crystal and found to be less than 2 ms. The contacts do not generate electrical signal under irradiation, as demonstrated in a different experiment using nonpyroelectric substrates such as glass.

**Calculation of Pyroelectric Coefficient. Case 1. Thick Homogeneous Crystal.** The pyroelectric current is proportional to the rate of temperature change:

$$I = \alpha A \frac{\partial T}{\partial t} \quad (1)$$

where  $\alpha$  is the pyroelectric coefficient of the crystal and  $A$  is the contact area. If a homogeneous plate-like crystal of a thickness  $d$  is subjected from a time moment  $t = 0$  to a homogeneous surface heat flux  $F_d$ , then for the period  $t < d^2/D$ , the current is constant and given by

$$I = \alpha A \frac{F_d}{C_v d} \quad (2)$$

where  $D$  is thermal diffusivity of the plate and  $C_v$  is the volume heat capacity.

**Case 2. Thin Homogeneous Crystal on a Conductive Holder.** If the sample is too thin to detect the current during the period  $t < d^2/D$ , but it is mounted on an electrically conductive holder of the thickness  $d_s$ , then for the time period  $1000d^2/D < (d + d_s)^2/D$ , the current is given by

$$I(t) = A\alpha F_d B(t)^{-1/2} \quad (3)$$

where  $B = (\pi\kappa_s C_s)^{-1/2}$  and  $\kappa_s$  and  $C_s$  are the holder's thermal conductivity and volume heat capacity, respectively.<sup>2</sup>

**Case 3. Thin Pyroelectric Layer on a Nonpyroelectric Electrically Insulating Crystal.** Thin pyroelectric layer on a nonpyroelectric electrically insulating crystal also generates pyroelectric current that decays with time proportionally to  $1/(t + t_0)^{1/2}$ . However, the analysis becomes somewhat more complicated.<sup>35</sup> Nevertheless, observation of a  $I(t) \propto 1/(t + t_0)^{1/2}$  dependence, as in DL-Ala, DL-Glu monohydrate, and DL-Ser, proves that the current originates from a thin pyroelectric layer present at the crystal surface.

**Computational Procedure for Estimating the Relative Layer, Attachment, and Binding Energies.** All energy computations were performed using Material Studio 6.1 package (Accelrys Inc. San Diego, CA) and the *Forcite* module. The energy expression was setup using the Dreiding force-field including hydrogen bond, van der Waals, and electrostatic contributions. Details of the computational method are given in the Supporting Information.

## ■ ASSOCIATED CONTENT

### S Supporting Information

Details of crystal growth, computational procedure for estimating the relative layer, attachment, and binding energies, and deuterium NMR procedure and results. This material is available free of charge via the Internet at <http://pubs.acs.org>.

## ■ AUTHOR INFORMATION

### Corresponding Authors

\*E-mail: Meir.Lahav@weizmann.ac.il

\*E-mail: Igor.Lubomirsky@weizmann.ac.il

### Notes

The authors declare no competing financial interest.

## ■ ACKNOWLEDGMENTS

The authors thank Drs. David Ehre and Silvia Piperno for discussions and Ido Azuri and Prof. Leeor Kronik for providing facilities for carrying out the computations. The authors express

their appreciation to the Israeli Science Foundation. This research is made possible in part by the historic generosity of the Harold Perlman Family.

## ■ REFERENCES

- (1) Lang, S. B. *Phys. Today* **2005**, *58*, 31.
- (2) Lubomirsky, I.; Stafudd, O. *Rev. Sci. Instrum.* **2012**, *83*, 1.
- (3) Piperno, S.; Mirzadeh, E.; Mishuk, E.; Ehre, D.; Cohen, S.; Eisenstein, M.; Lahav, M.; Lubomirsky, I. *Angew. Chem., Int. Ed.* **2013**, *52*, 6513.
- (4) Frenkel, A. I.; Ehre, D.; Lyahovitskaya, V.; Kanner, L.; Wachtel, E.; Lubomirsky, I. *Phys. Rev. Lett.* **2007**, *99*, No. 215502.
- (5) Frenkel, A. I.; Feldman, Y.; Lyahovitskaya, V.; Wachtel, E.; Lubomirsky, I. *Phys. Rev. B* **2005**, *71*, No. 024116.
- (6) Ehre, D.; Lyahovitskaya, V.; Tagantsev, A.; Lubomirsky, I. *Adv. Mater.* **2007**, *19*, 1515.
- (7) Wachtel, E.; Lubomirsky, I. *Adv. Mater.* **2010**, *22*, 2485.
- (8) Batagianis, A.; Wubbenhorst, M.; Hulliger, J. *Curr. Opin. Solid State Mater. Sci.* **2010**, *14*, 107.
- (9) Behrnd, N. R.; Couderc, G.; Wubbenhorst, M.; Hulliger, J. *Phys. Chem. Chem. Phys.* **2006**, *8*, 4132.
- (10) Gervais, C.; Hulliger, J. *Cryst. Growth Des.* **2007**, *7*, 1925.
- (11) Destro, R.; Marsh, R. E.; Bianchi, R. *J. Phys. Chem.* **1988**, *92*, 966.
- (12) Shimon, L. J. W.; Vaida, M.; Addadi, L.; Lahav, M.; Leiserowitz, L. *J. Am. Chem. Soc.* **1990**, *112*, 6215.
- (13) Weissbuch, I.; Kuzmenko, I.; Vaida, M.; Zait, S.; Leiserowitz, L.; Lahav, M. *Chem. Mater.* **1994**, *6*, 1258.
- (14) Kwok, R. S.; Maxton, P.; Migliori, A. *Solid State Commun.* **1990**, *74*, 1193.
- (15) Towler, C. S.; Davey, R. J.; Lancaster, R. W.; Price, C. J. *J. Am. Chem. Soc.* **2004**, *126*, 13347.
- (16) Weissbuch, I.; Leiserowitz, L.; Lahav, M. *Cryst. Growth Des.* **2006**, *6*, 625.
- (17) Minkov, V. S.; Chesalov, Y. A.; Boldyreva, E. V. *J. Struct. Chem.* **2010**, *51*, 1052.
- (18) Lima, J. A.; Freire, P. T. C.; Melo, F. E. A.; Mendes, J.; De Sousa, G. P.; Lima, R. J. C.; Facanha, P. F.; Bordallo, H. N. *J. Raman Spectrosc.* **2010**, *41*, 808.
- (19) Han, G. J.; Chow, P. S.; Tan, R. B. H. *Cryst. Growth Des.* **2011**, *11*, 3941.
- (20) Lechuga-Ballesteros, D.; Rodriguez-Hornedo, N. *Pharm. Res.* **1993**, *10*, 1008.
- (21) Addadi, L.; Berkovich-Yellin, Z.; Weissbuch, I.; Lahav, M.; Leiserowitz, L.; Weinstein, S. *J. Am. Chem. Soc.* **1982**, *104*, 2075.
- (22) Wang, H. F.; Bell, R. C.; Iedema, M. J.; Schenter, G. K.; Wu, K.; Cowin, J. P. *J. Phys. Chem. B* **2008**, *112*, 6379.
- (23) Independent support for the occurrence of induced local polar disorder by the guest molecules is provided by independent density functional studies on related systems currently in progress by Ido Azuri and Prof Leeor Kronik, private communication.
- (24) Vaida, M.; Shimon, L. J. W.; Weisinger-Lewin, Y.; Frolow, F.; Lahav, M.; Leiserowitz, L.; McMullan, R. K. *Science* **1988**, *241*, 1475.
- (25) Vaida, M.; Shimon, L. J. W.; van Mil, J.; Ernst-Cabrera, K.; Addadi, L.; Leiserowitz, L.; Lahav, M. *J. Am. Chem. Soc.* **1989**, *111*, 1029.
- (26) McBride, J. M.; Bertman, S. B. *Angew. Chem., Int. Ed.* **1989**, *28*, 330.
- (27) Weisinger-Lewin, Y.; Frolow, F.; McMullan, R. K.; Koetzle, T. F.; Lahav, M.; Leiserowitz, L. *J. Am. Chem. Soc.* **1989**, *111*, 1035.
- (28) Kahr, B.; McBride, J. M. *Angew. Chem., Int. Ed.* **1992**, *31*, 1.
- (29) Berkovich-Yellin, Z.; Addadi, L.; Idelson, M.; Leiserowitz, L.; Lahav, M. *Nature* **1982**, *296*, 27.
- (30) Berkovich-Yellin, Z. *J. Am. Chem. Soc.* **1985**, *107*, 8239.
- (31) Hod, I.; Mastai, Y.; Medina, D. D. *CrystEngComm* **2011**, *13*, 502.
- (32) Viedma, C. *Origins Life Evol. Biospheres* **2001**, *31*, 501.
- (33) Lee, T.; Lin, Y. K. *Cryst. Growth Des.* **2010**, *10*, 1652.
- (34) Chynoweth, A. G. *J. Appl. Phys.* **1956**, *27*, 78.

(35) Ehre, D.; Mirzadeh, E.; Stafsudd, O.; Lubomirsky, I. 2014,  
Accepted for publication in *Ferroelectrics*.